Electronic Supplementary Material (ESI) for ChemComm.

Supporting Information:

Room temperature solid-state deformation induced high-density lithium grain boundaries to enhance the cycling stability of lithium metal batteries

Zhang Xue-Ying [1], Zhang Yong [1]*, Gao Yong [2], Zhao Hong[1],*

[1] *Department of Materials Science and Engineering, Dalian Jiaotong University, Dalian 116028, Liaoning, China*

[2] *Institute of Science and Technology for New Energy, Xi'an Technological University, Xi'an 710021, Shannxi, China*

*Corresponding author.

E-mail: zhaohong@djtu.edu.cn (Zhao Hong)

*Corresponding author.

E-mail: zhangyong@126.com (Zhang Yong)

Experimental procedure

Solid-state growth of high-density nanograin boundaries on the surface of lithium anode substrate was performed by a repeated grinding process under room temperature. Firstly, lithium foil of 0.3 mm thickness was repeatedly grinded for 15 minutes by a mortar grinder (RM 200) in an argon-filled glove box, in which the rotational speed was 100 rpm (Fig. S1). Hereafter, the original ungrinded lithium foils and grinded lithium foils are named as UG-Li and G-Li, respectively. Subsequently, the morphologies of UG-Li and G-Li samples were observed by scanning electron microscopy (SEM, SUPRA55). In addition, the crystallographic structures of UG-Li and G-Li samples were tested by an X-ray diffraction (XRD, D/Max-Ultima+) with Cu Kα radiation at a scan speed of 6 ° min^{-1}. Moreover, the samples were characterized by transmission electron microscopy (TEM, JEOL 2010F). For accuracy, the original tested XRD patterns of UG-Li and G-Li samples were corrected by subtracting the background. To prevent chemical oxidation of UG-Li and G-Li samples by water and oxygen molecules in atmosphere, an argon-filled sample-transferring chamber was adopted to transfer UG-Li and G-Li samples from argon-filled glove box to the sample-chambers of SEM, XRD and TEM characterization.

All 2032-type coin cells were assembled in an argon-filled glove box, in which the $LiPF_6$ in EC and DEC mixed solution (1:1) was employed as electrolyte. Firstly, graphite electrode, silicon electrode and $LiFePO_4$ electrode were fabricated by a coating method. The active materials (graphite, silicon or $LiFePO_4$) were blended with polyvinylidene fluoride (PVDF) binder to form slurry product. Then, the slurry of active materials was coated on copper foil, which was dried at 120 ℃ for 12 hours in a vacuum oven. The loading capacity of graphite and Si electrode sheets is 1 mg/cm^2. And the loading capacity of $LiFePO_4$ electrode is 10 mg/cm^2. Subsequently, UG-Li||graphite, G-Li||graphite, UG-Li||Si and G-Li||Si batteries are assembled, and the batteries were charged and discharged at a constant current of 0.05 mA on the LAND system. UG-Li||$LiFePO_4$ and G-Li||$LiFePO_4$ were charged and discharged at a constant current of 1.5 mA/cm^2 on the LAND system. The discharge and charge capacities of UG-Li||graphite, G-Li||graphite, UG-Li||$LiFePO_4$, G-Li||$LiFePO_4$, UG-Li||Si and G-Li||Si batteries were calculated by the total capacity of battery (mAh)/mass of active material in cathode (g). In addition, UG-Li||UG-Li and G-Li||G-Li symmetric batteries were assembled to evaluate the cycle stability of lithium electrodes. The test conditions were 0.5 mA constant current charge and discharge for one hour as one cycle.

In order to analyze the kinetic performance of lithium metal batteries, UG-Li||Si and G-Li||Si batteries were tested by cyclic voltammogram (CV) and electrochemical impedance spectroscopy (EIS) using Shanghai Chen-hua electrochemical workstation. The scanning speed of CV tests was 0.1 mV/s and the scanning

voltage range was 0.01-2 V (vs. Li/Li^+). EIS tests were carried out in the range of was 10 mHz-1000 kHz an d the scanning speed was 5 mV/s.

Calculation method

The adsorption and deposition behavior of Li ions on lithium nanograin boundaries was performed by density-functional theory (DFT), which was implemented in the Vienna ab initio simulation package (VAS P) code. The exchange correlation energies of electron-ion reactions were described within the generalized gradient approximation (GGA) as parameterized by Perdew, Burke, and Ernzerhof provided in VASP datab ase.[1] The Monkhorst-Pack method with a 9×9×9 k-point grid sampling in the Brillouin zone is adopted, and the plane-wave energy cut-off is 300 eV. The adsorption energies of Li ions on lithium nanograin boundarie s were defined as follows:

$$E_{ads} = E(GB/Li) - E(GB) - E(Li) \qquad (1)$$

Where, Eads was adsorption energies of Li ion on lithium grain boundaries. Moreover, E(GB/Li) was the fr ee energy when Li ion was adsorbed on lithium nanograin boundaries. E(GB) and E(Li) were the free energ ies of lithium nanograin boundaries and Li ion, respectively. For accuracy, the adsorption energies of Li ion adsorption on both surfaces of all the lithium nanograin boundaries were calculated.

The periodically repeated Li(110), Li(200), Li(211) and lithium nanograin boundaries surface slabs we re generated with supercell units of 3×3×1. To avoid periodic interactions, the vacuum layers of 15 Å were added into the z direction of Li(110), Li(200), Li(211) and lithium grain boundaries surface slabs. Furtherm ore, Bader charge calculation was conducted to estimate the distribution of electronic charges on Li(110), L i(200), Li(211) and lithium nanograin boundaries.

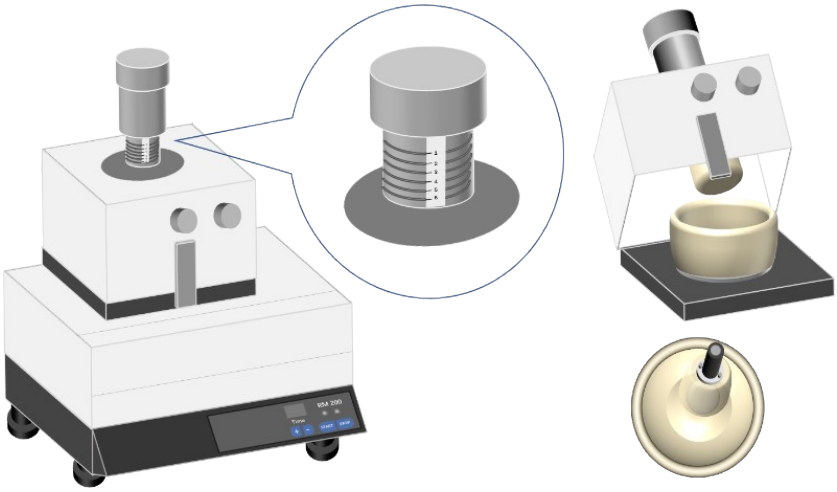

Fig. S1 Schematic illustration of a mortar grinder (RM 200)

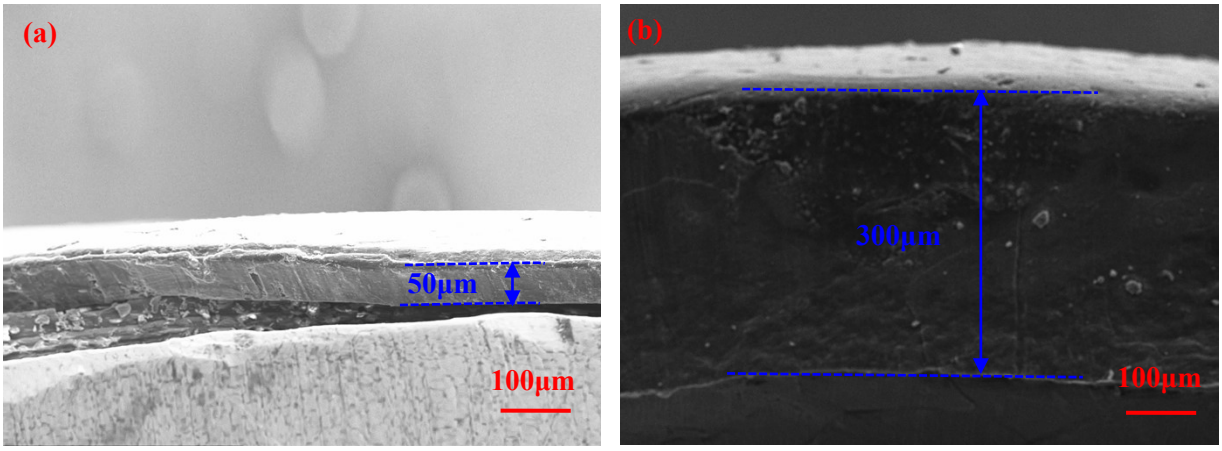

Fig. S2 Cross-sectional SEM observation of G-Li anode (a) and UG-Li anode (b) before cycling

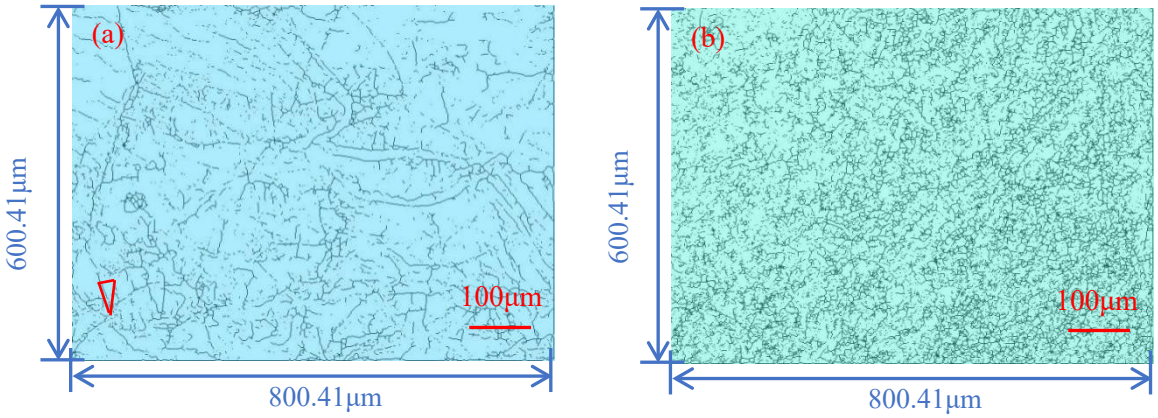

Fig. S3 Measurement of lithium grain boundary densities for UG-Li (a) and G-Li (b) anodes by a quantitative metallography method.

The grain boundary densities of UG-Li and G-Li anodes are calculated according to the following equation:

$$A = L/S$$

Where, A is grain boundary density, while L is the sum length of all grain boundaries within the measurement range and S is the area of measured images. Firstly, the area of image (a) or image (b) is measured, which is 480572.6 μm^2. Secondly, it is measured that the sum length of grain boundaries for UG-Li anode in Fig. S3(a) is 2448.0 μm, and the sum length of grain boundaries for G-Li anode in Fig. S3(b) is 56865.4 μm. Finally, the grain boundary density of UG-Li anode in Fig. S3(a) is calculated to be 0.0297 μm^{-1}, i.e. 5.09 nm^{-1}, and the grain boundary density of G-Li anode in Fig. S3(b) is 0.1183 μm^{-1}, i.e. 118.3 nm^{-1}.

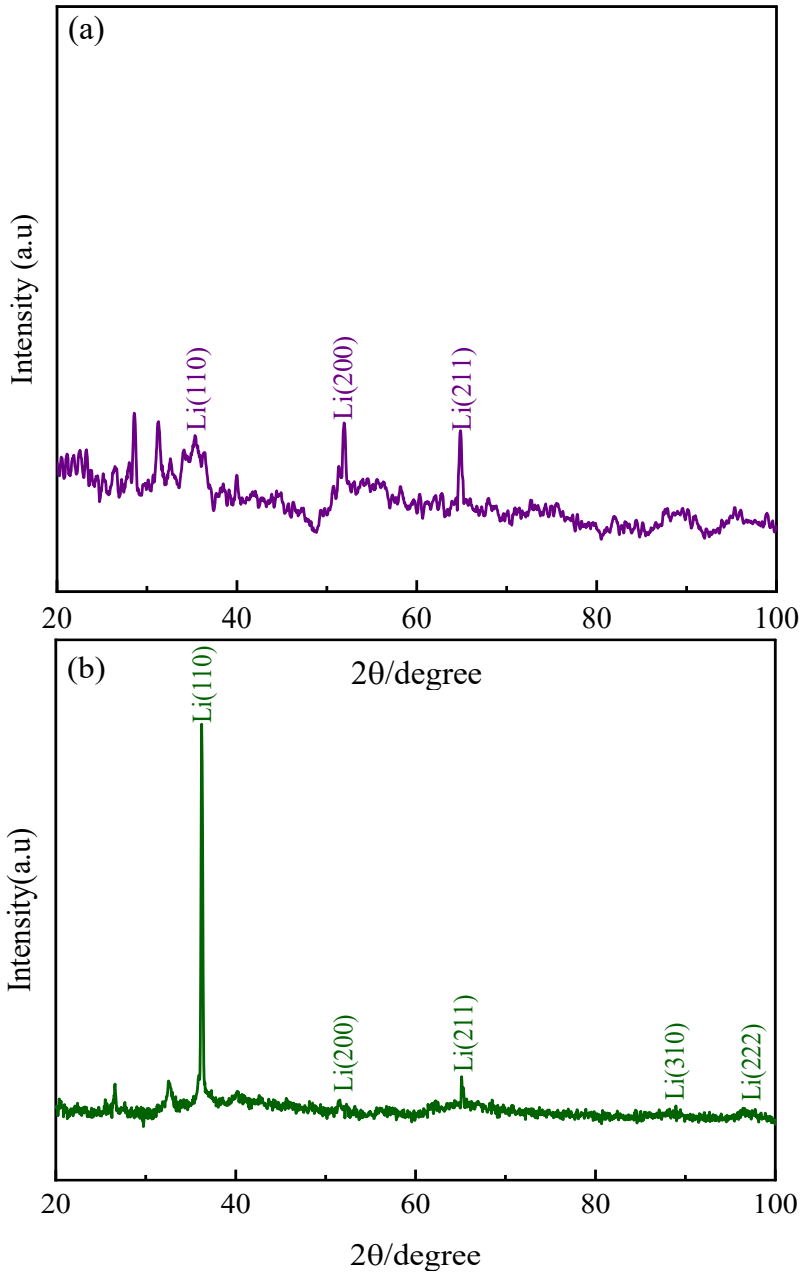

Fig. S4 XRD patterns of UG-Li (a) and G-Li (b) anodes

In the case of UG-Li, there are three peaks at 36.3 °, 51.9 ° and 64.4 °, corresponding to Li(110), Li(200) and Li(211) planes, respectively (JCJPDS card, No. 00-015-0401). Compared to UG-Li, the intensity of Li(110) is obviously increased in G-Li anode, indicating obvious plastic deformation of lithium metal along Li(110) plane under continuous grinding process.

Accordingly, abundant grain boundaries of Li(110), Li(200) and Li(211) crystal planes are created.

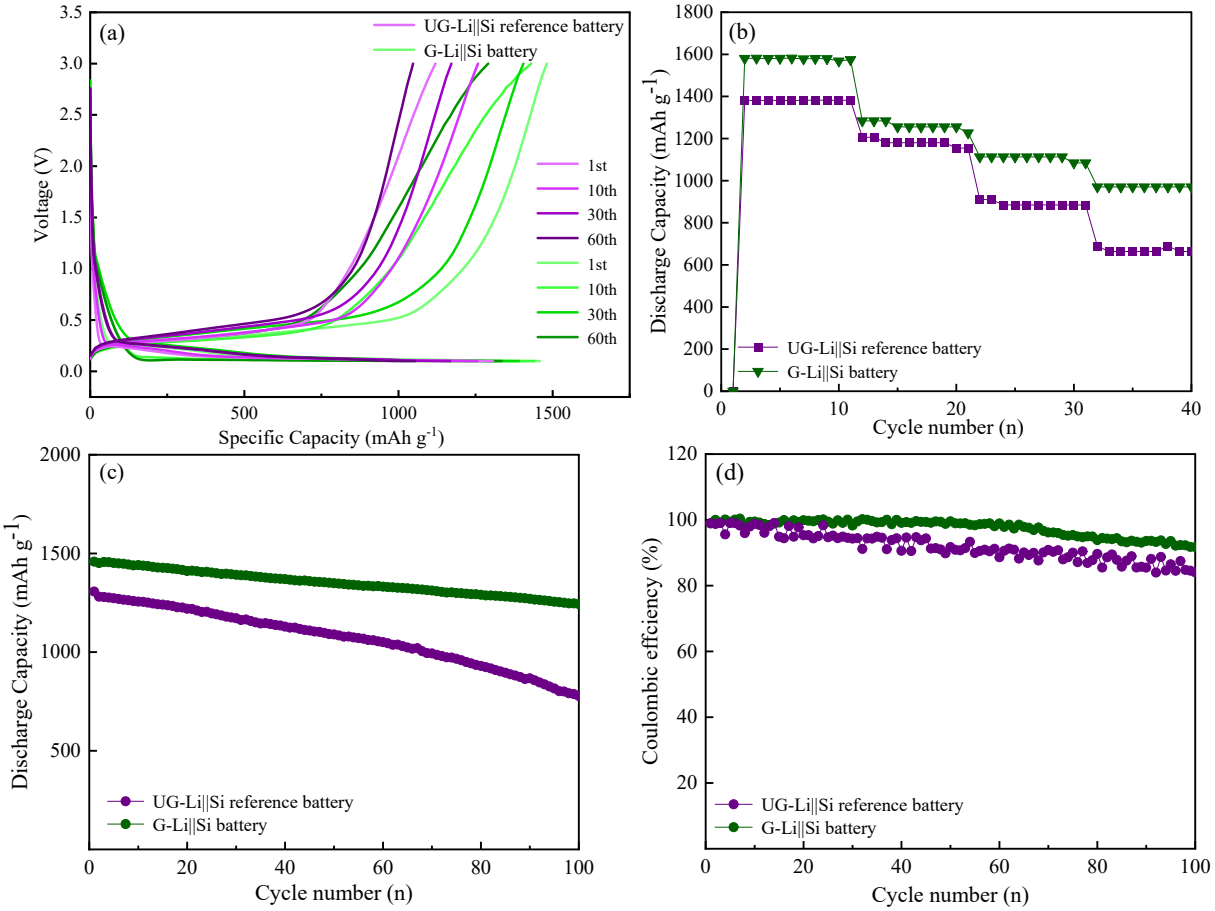

Fig. S5. Electrochemical performances testing of Li||Si batteries

(a) Capacity-voltage curves of UG-Li||Si and G-Li||Si batteries; (b) Rate capacity curves of UG-Li||Si and G-Li||Si batteries; (c) Cycling performances of UG-Li||Si and G-Li||Si batteries; (d) Columbic efficiencies of UG-Li||Si and G-Li||Si batteries;

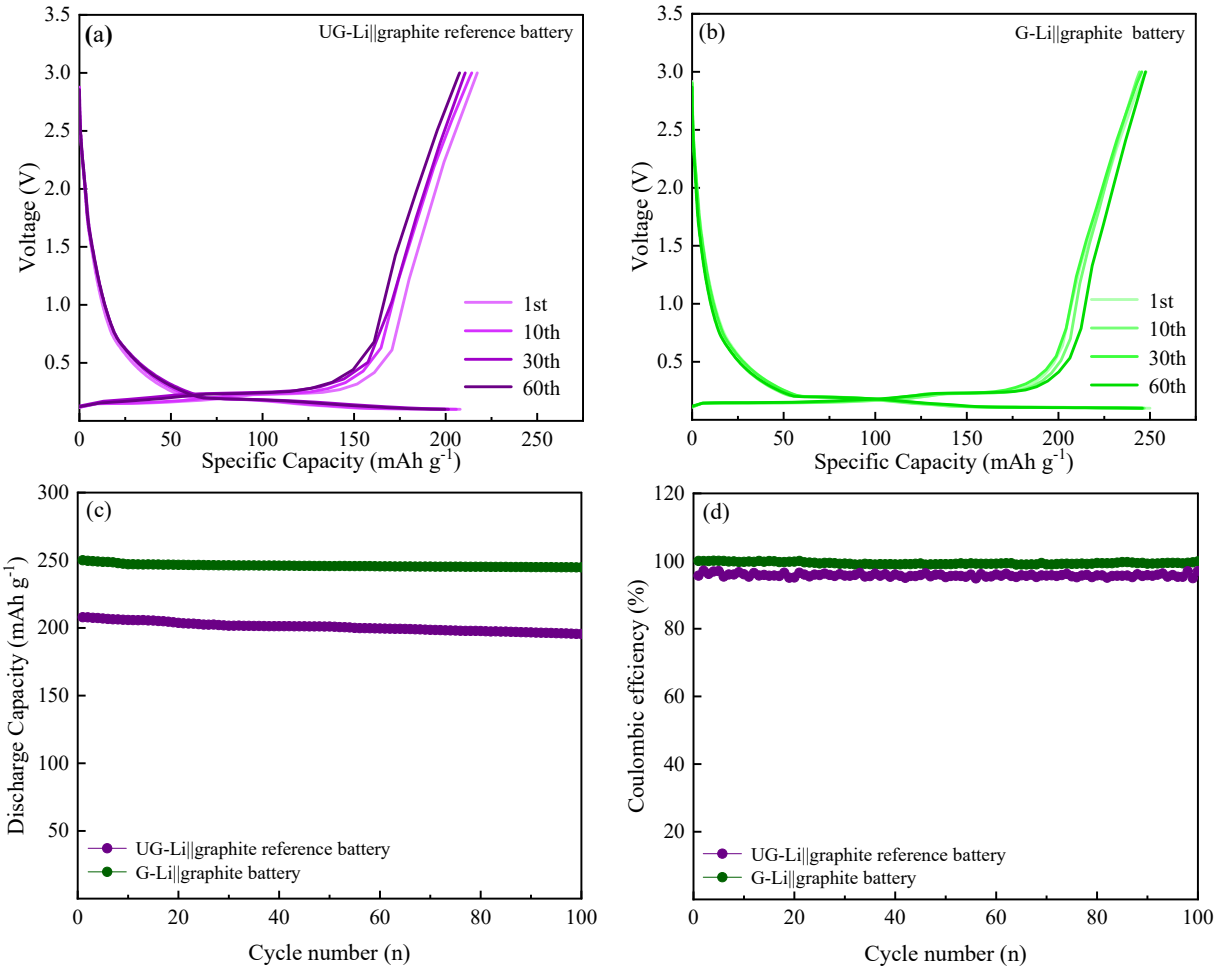

Fig. S6. Electrochemical performances testing of Li||graphite batteries

(a) Capacity-voltage curves of UG-Li||graphite batteries;

(b) Capacity-voltage curves of G-Li||graphite batteries;

(c-d) Cycling performances of UG-Li||graphite and G-Li||graphite batteries

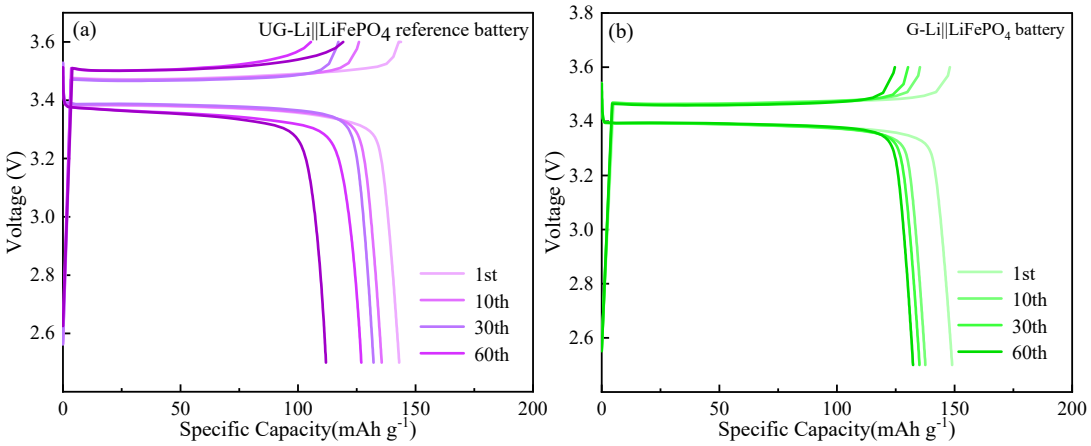

Fig. S7 Electrochemical performances testing of Li||$LiFePO_4$ batteries

(a) Capacity-voltage curves of UG-Li||$LiFePO_4$ batteries;

(b) Capacity-voltage curves of G-Li||$LiFePO_4$ batteries.

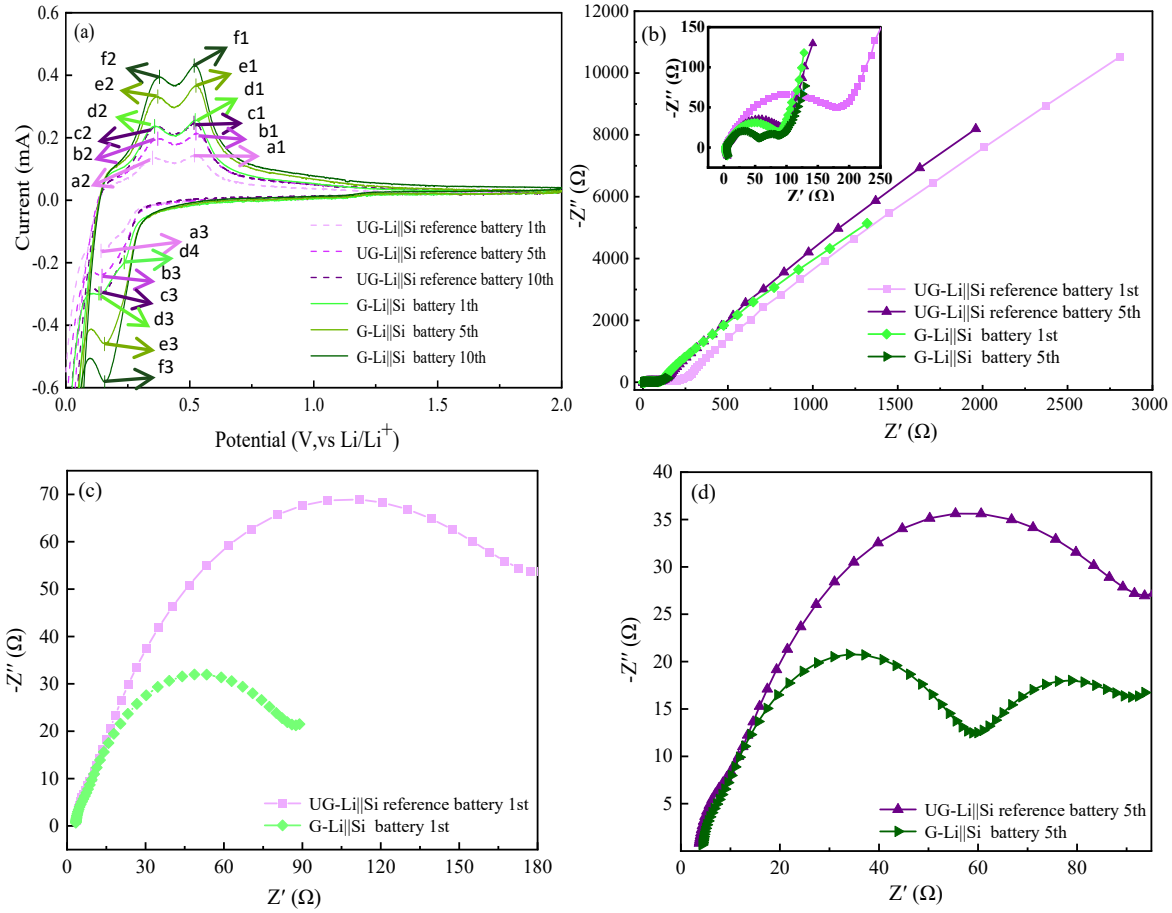

Fig. S8 CV and EIS testing of UG-Li||Si and G-Li||Si batteries. a, CV curves of UG-Li||Si and G-Li||Si batteries. b, EIS curves of UG-Li||Si and G-Li||Si batteries after 10th cycles. c–d, Nyquist plots of UG-Li||Si and G-Li||Si batteries after 1st (c) and 5th (d) cycles.

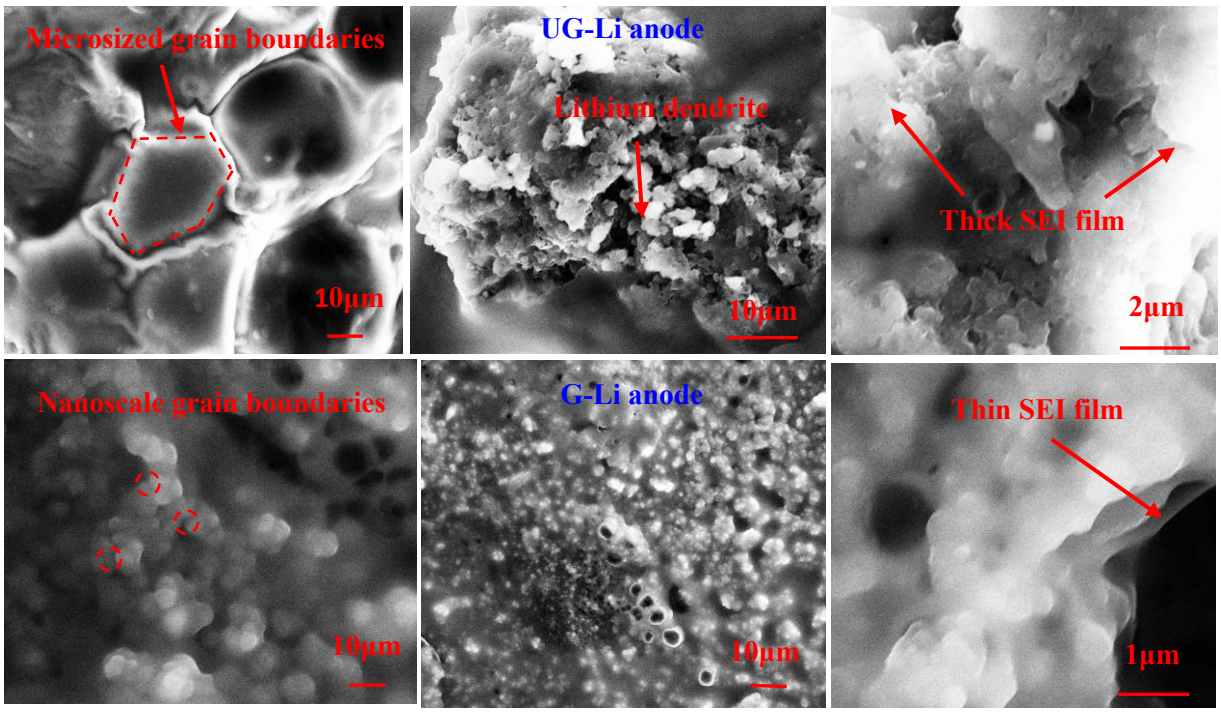

Fig. S9 the insets are SEM observation of UG-Li and G-Li anodes

after 100th plating/stripping cycles, respectively

Table S1 The CV peaks of UG-Li||Si and G-Li||Si batteries

UG-Li||Si reference battery 1st	**a**	**a1: 0.350**	**a2: 0.519**	**a3: 0.142**	**-**
UG-Li||Si reference battery 5th	**b**	**b1: 0.371**	**b2: 0.525**	**b3: 0.146**	**-**
UG-Li||Si reference battery 10th	**c**	**c1: 0.358**	**c2: 0.517**	**c3: 0.142**	**-**
G-Li||Si battery 1st	**d**	**d1: 0.358**	**d2: 0.522**	**d3: 0.142**	**d4: 0.238**
G-Li||Si battery 5th	**e**	**e1: 0.371**	**e2: 0.525**	**e3: 0.156**	**-**
G-Li||Si battery 10th	**f**	**f1: 0.378**	**f2: 0.518**	**f3: 0.157**	**-**

In reference of previous reports,[2, 3] the reduction peaks of 0.14-0.15V are related to lithiation of Li ions into silicon electrode, and the oxidation peaks (0.35V and 0.51V) are attributed to de-lithiation of Li ions from silicon electrode. During the first discharge reaction of G-Li||Si battery, the only reduction peak of d4 at 0.238 V indicates the formation of SEI film during the first discharge process of G-Li electrode.

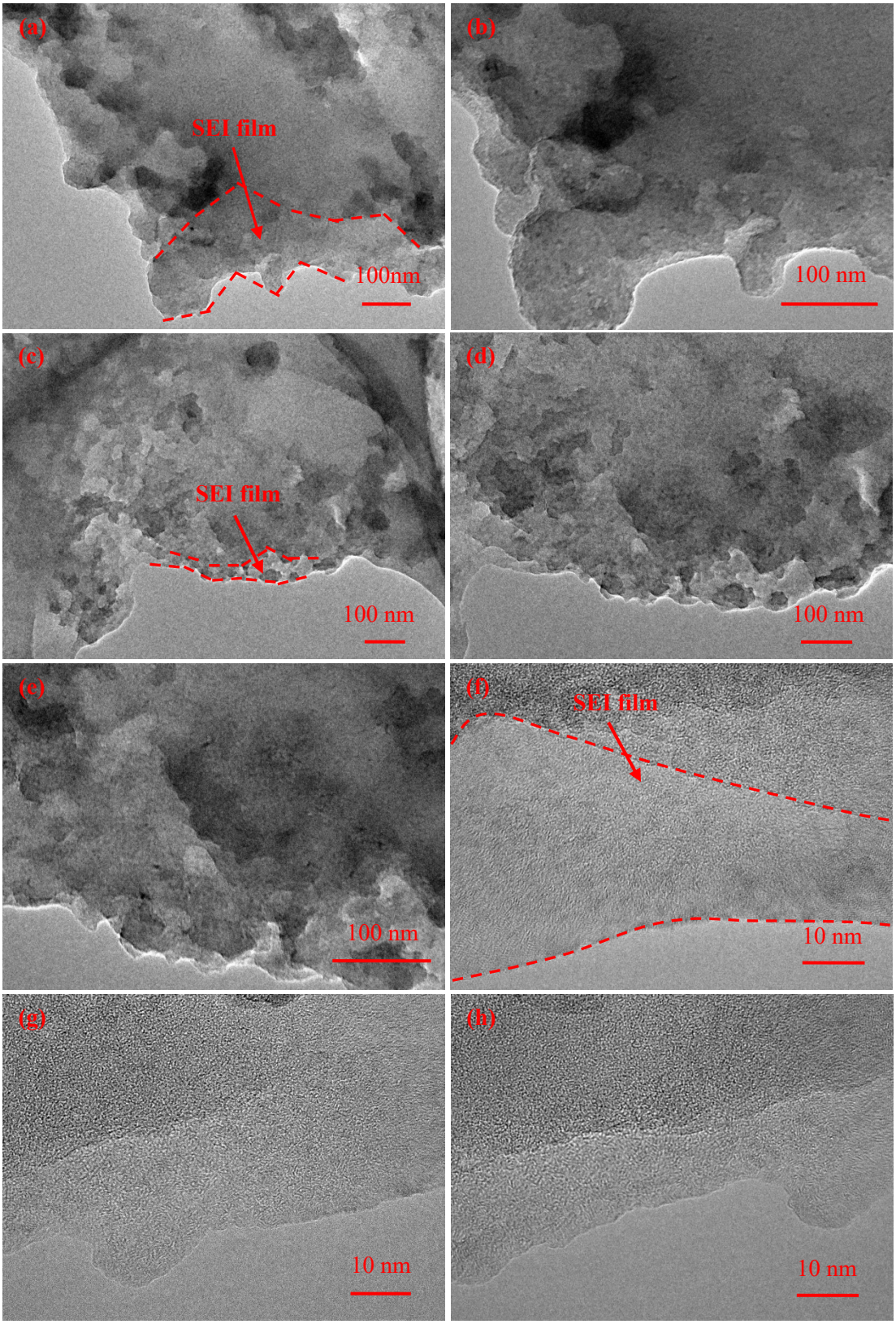

Fig. S10: TEM characterization of SEI films in UG-Li (a-b) and G-Li (c-h) anodes after 100th plating/stripping cycle

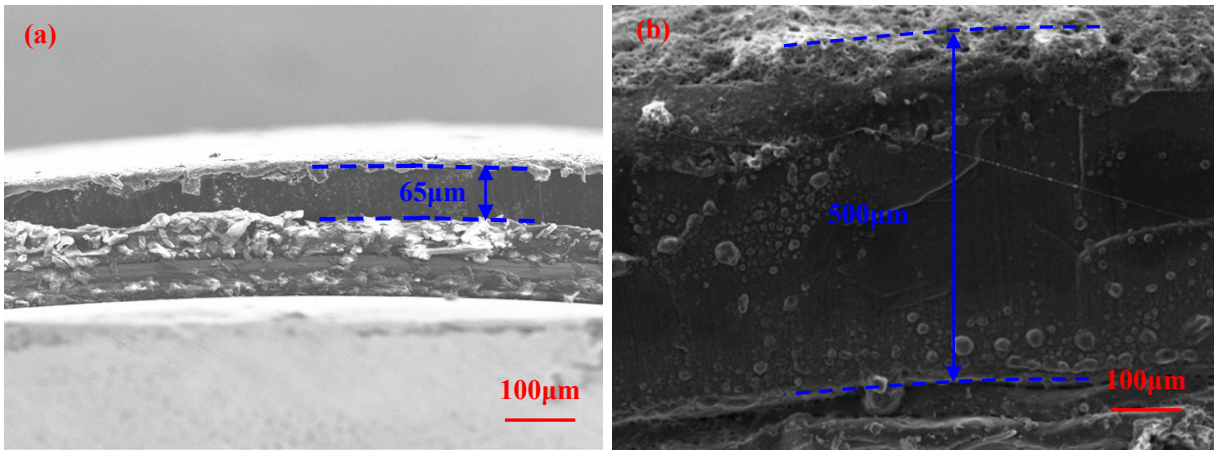

Fig. S11 Cross-sectional SEM observation of G-Li anode (a) and UG-Li anode (b) after 100th plating/stripping cycles.

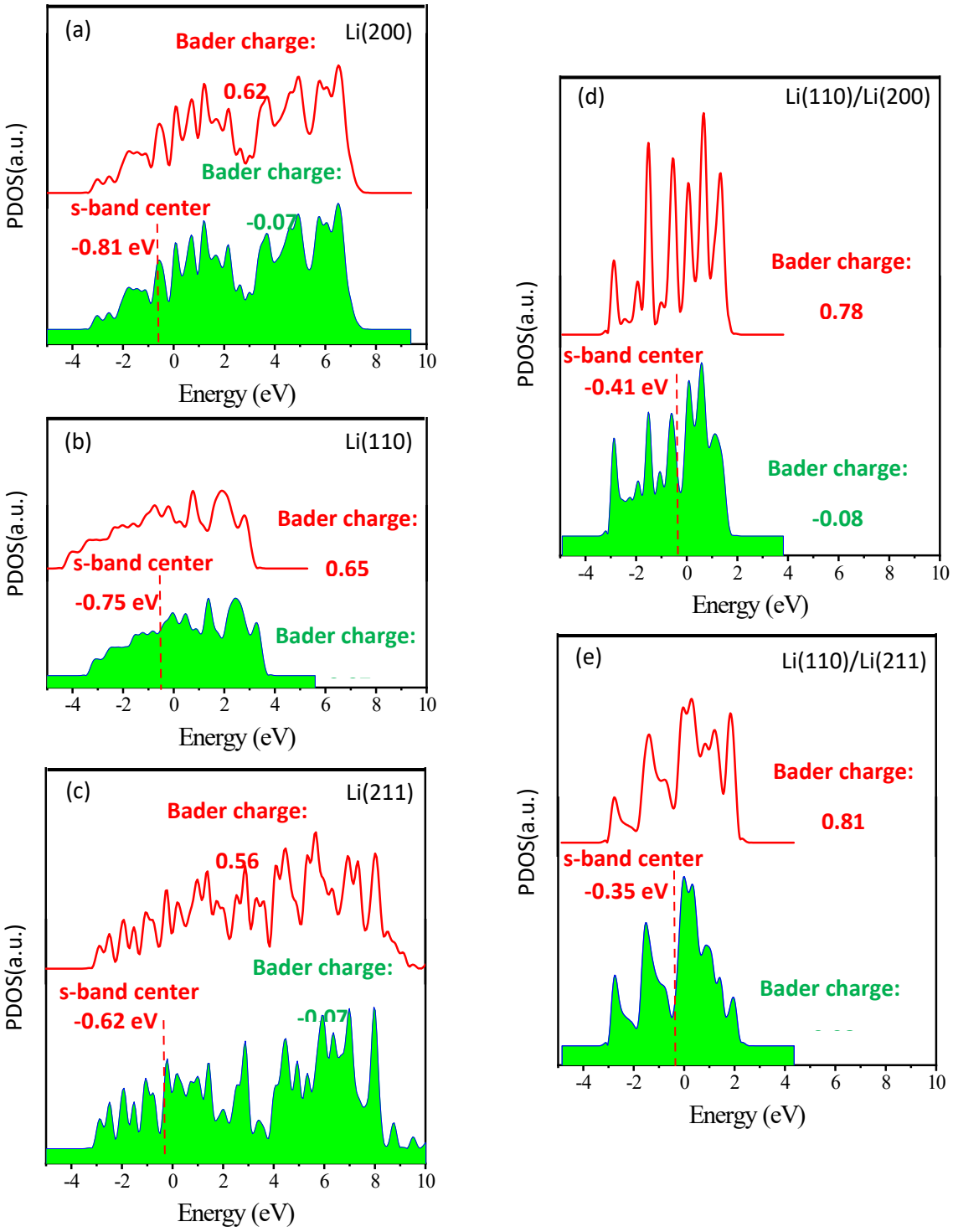

Fig. S12: PDOS, Bader charge and s-band center of Li ion adsorption on Li(200), Li(110), Li(211), Li(110)/Li(200) and Li(110)/Li(211) grain boundaries, respectively.

Where, the red line is adsorbed Li ion, and the green lines are corresponded to Li atoms of Li(110), Li(200), Li(211), Li(110)/Li(200) and Li(110)/Li(211) grain boundaries, respectively.

References

[1] J.P. Perdew, K. Burke, M. Ernzerhof. Phys. Rev. Lett., 1996, 77, 3865.
[2] Q. Zhang, Y.X. Yu, H.J. Li, F.Y. Zhang, Y.D. Liu, Electrochim. Acta, 2023, 466, 142991.
[3] T. Mu, Y.P. Sun, C.H. Wang, Y. Zhao, K. Doyle-Davis, J.N. Liang, X.L. Sui, R.Y. Li, C.Y. Du, P.J. Zuo, G.P. Yin, X.L. Sun, Nano Energy, 2022, 103, 107829.